Effects of Notch signaling on proliferation, angiogenesis, and adipogenesis of hemangioma-derived stem cells

Weidong Wang, Sheng Chen, Yuan Wang, Jie Cui, Weimin Shen

Department of Burns and Plastic Surgery, Children's Hospital of Nanjing Medical University, Nanjing, Jiangsu, China

ABSTRACT

Hemangioma-derived stem cells (Hem-SCs) constitute the cellular basis for adipogenesis during infantile hemangioma (IH) regression, with Notch signaling implicated in this process. To elucidate Notch's role in Hem-SCs biology, we isolated primary Hem-SCs from proliferative-phase IH specimens and validated their stem cell characteristics. Three days post-intervention with the γ-secretase inhibitor DAPT (N-[N-(3,5-difluorophenacetyl)-L-alanyl]-S-phenylglycine t-butylester), we assessed Notch and PI3K/AKT signaling dynamics while concurrently measuring vascular endothelial growth factor receptor (VEGFR) protein expression. Cellular proliferation was quantified *via* CCK-8 assay. During adipogenic differentiation (Day 14), RTqPCR evaluated Notch pathway genes (*Notch1*, *Jagged1*, *Hes1*), while adipogenic commitment was determined through Oil Red O staining and adipocyte-specific gene expression (PPARγ, C/EBPα). We demonstrate that DAPT suppresses Notch and PI3K/AKT signaling in Hem-SCs, concomitantly enhancing cellular proliferation and angiogenesis. Simultaneous analysis of VEGFR expression revealed differential DAPT-mediated regulation: VEGFR1 downregulation with concomitant VEGFR2 upregulation. During adipogenic induction, Notch pathway genes (*Notch1, Jagged1, Hes1*) were significantly downregulated. DAPT treatment further elevated adipogenic markers (PPARγ, C/EBPα) and lipid accumulation. Crucially, co-administration of the PI3K activator 740Y-P reversed DAPT-induced adipogenesis. Mechanistically, Notch inhibition promotes Hem-SCs proliferation, angiogenesis, and adipocyte differentiation by attenuating PI3K/AKT signaling.

Key words: infantile hemangioma; hemangioma-derived stem cells; proliferation; adipogenic differentiation; Notch.

Correspondence: Weimin Shen, Department of Burns and Plastic Surgery, Children's Hospital of Nanjing Medical University, 72 Guangzhou Road, Nanjing, Jiangsu 210008, China. E-mail: swmswmswm@sina.com

Contributions: WW, SC, study design; YW, SC, research performing; WW, data analysis, manuscript original drafting; WW, JC, clinical samples and data collection; WS, JC, technical assistance; WS, financial support, manuscript revision. All the authors read and approved the final version of the manuscript and agreed to be accountable for all aspects of the work.

Conflict of interest: the authors declare that no conflict of interest, and all authors confirm accuracy.

Ethics approval and consent to participate: the protocol of this study was approved by the Ethics Committee of Children's Hospital of Nanjing Medical University (approval no. 201902068-1; Nanjing, China) in accordance with the Helsinki Declaration of 1975, as revised in 2013. Written informed consent was obtained from all patients or their legal guardians.

Availability of data and materials: the datasets generated during and/or analyzed during the current study are available from the corresponding author on reasonable request.

Funding: the current study was supported by the Science and Technique Development Foundation of Nanjing Medical University (NMUB2020088).

Introduction

Infantile hemangioma (IH), the most common benign soft-tissue tumor in infants, affects 5-10% of this population.[1,2] Clinically, IH manifests within the first postnatal week, undergoes rapid proliferation during the initial 6 months, and subsequently enters an involution phase characterized by gradual size reduction over the following year. While most lesions fully regress by early childhood (6-8 years), residual cutaneous changes -including textural abnormalities, dyschromia, and fibrofatty tissue deposition- frequently persist, potentially resulting in scarring with cosmetic implications. When involving critical anatomical sites (*e.g.*, periorbital, airway) or presenting with large-volume lesions, IH may cause destructive local effects including tissue compression, ulceration, recurrent infections, and end-organ damage. Such high-risk IH carries significant life-threatening potential, necessitating therapeutic intervention to accelerate involution and mitigate complications.[3,4]

The molecular mechanisms underlying IH regression remain incompletely elucidated. Adipogenesis occurring during the involution phase may represent a key contributor to this process.[5,6] Notably, clinical observations of increased adipose deposition following β-blocker therapy (*e.g.,* propranolol) for IH provide supporting evidence for this adipogenic hypothesis.

Stem cells (SCs) are pluripotent cells with multilineage differentiation potential.[7] Hemangioma-derived SCs (Hem-SCs), isolated from IH, represent a subtype of SCs. They exhibit multilineage differentiation capacity and can be induced to differentiate into diverse cell types -including chondrocytes, osteoblasts, and adipocytes- under specific conditions.[8] Furthermore, Hem-SCs highly express multiple pro-angiogenic factors and critically contribute to IH angiogenesis. Collectively, these properties suggest that Hem-SCs may constitute the cellular basis for pathological changes during IH proliferation and regression.

Vascular endothelial growth factor (VEGF) is a key cytokine regulating the proliferation, differentiation, and maturation of vascular endothelial cells, with a critical role in angiogenesis.[9] The VEGF receptor family comprises five subtypes: VEGFR1 (Flt-1), VEGFR2 (KDR/Flk-1), VEGFR3 (Flt-4), neuropilin-1 (NRP1), and neuropilin-2 (NRP2). Among these, VEGFR1 and VEGFR2 are predominantly expressed on vascular endothelial cells and serve as primary VEGF receptors, whereas VEGFR3 localizes to lymphatic endothelial cells and specific capillary subtypes. Ligand binding to VEGFR2 promotes vascular endothelial cell proliferation and angiogenesis. Conversely, VEGFR1 activation antagonizes VEGFR2-mediated proliferative signaling.[10,11] Consequently, the differential regulation of VEGFR1 and VEGFR2 significantly influences vascular pathogenesis in IH.

The Notch signaling pathway is an evolutionarily conserved intercellular communication system that critically regulates cellular proliferation and differentiation. This pathway comprises three core components: receptors, ligands, and intracellular effector molecules. In mammals, Notch signaling involves four receptors (Notch1-4) and five canonical ligands (Jagged1, Jagged2, Delta-like 1, Delta-like 3, Delta-like 4).[12,13] Notably, transcriptomic analyses reveal elevated expression of Notch pathway genes during the regression phase of IH compared to the proliferative phase.[14] This differential expression profile suggests Notch signaling may actively promote IH regression.

The PI3K/AKT signaling pathway orchestrates critical cellular processes including proliferation, apoptosis, metabolism, and angiogenesis.[15] This evolutionarily conserved cascade comprises phosphatidylinositol 3-kinase (PI3K) and its downstream effector serine/threonine kinase AKT (protein kinase B). The cell-permeable phosphopeptide 740Y-P serves as a potent PI3K activator that potentiates PI3K/AKT signaling.[16] Accumulating evidence implicates PI3K/AKT dysregulation in IH pathogenesis, with emerging studies revealing crosstalk between Notch and PI3K/AKT pathways.[17,18] Mechanistically, Notch signaling activates PI3K/AKT through suppression of phosphatase and tensin homolog (PTEN) phosphorylation.[19] However, at present, it is unclear whether the Notch pathway and PI3K/AKT/mTOR pathway, crucial for cell growth and proliferation regulation, have a special relationship in IH. This is worth further study.

In this study, we investigated the functional consequences of Notch signaling perturbation in cultured Hem-SCs. Our findings demonstrate that Notch pathway modulation directly regulates Hem-SCs proliferation, angiogenic capacity, and adipogenic differentiation. Mechanistically, we identified crosstalk between Notch and PI3K/AKT signaling, revealing a novel axis controlling Hem-SCs fate. These insights provide a therapeutic framework for targeted hemangioma intervention.

Materials and Methods

Preparation of hemangioma specimens

Hemangioma specimens were obtained from 10 IH cases (Figure 1a) treated in the Department of Burns and Plastic Surgery at the Children's Hospital of Nanjing Medical University (Nanjing, China) between May 2021 and August 2021, with a mean age of 3.6 (range, 2-6) months. All postoperative pathology reported IH of the proliferative stage (Figure 1b). The protocol of this study was approved by the Ethics Committee of Children's Hospital of Nanjing Medical University (approval no. 201902068-1; Nanjing, China) in accordance with the Helsinki Declaration of 1975, as revised in 2013. Written informed consent was obtained from all patients or their legal guardians.

Isolation and identification of Hem-SCs

Fresh hemangioma specimens were collected. The skin and adipose tissues were removed, and the hemangioma tissues were cut into pieces; 0.2% collagenase A (Serva Electrophoresis GmbH, Heidelberg, Germany) was then added and the tissues were digested at 37°C in a water bath for 2 h. When the tissue mass was dispersed into single cells or small cell masses, low glucose Dulbecco's modified Eagle's medium (DMEM, ThermoFisher Scientific, Waltham, MA, USA) and 10% fetal bovine serum (FBS, HyClone, Logan, UT, USA) were added. The single-cell suspension was obtained by filtration with a 70-μm mesh. Then, red blood cell lysate (Beyotime Biotechnology, Haimen, China) was added, and the mixture was centrifuged. The supernatant was discarded, and the pellet was resuspended in DMEM supplemented with 10% FBS. $CD133^+$ cells were isolated from the single-cell suspension via magnetic-activated cell sorting (Miltenyi Biotec, Inc., Auburn, CA, USA) using anti-CD133 microbeads. Cells were cultured on fibronectin-coated plates (5 μg/cm²) in endothelial growth medium-2 (EGM-2; Lonza Group, Ltd., Basel, Switzerland) supplemented with 20% FBS and 1% penicillin/streptomycin (HyClone). Cultures were maintained at 37°C in a humidified 5% CO_2.

The primary cells were passaged according to 1:2. We have observed the obtained Hem-SCs cells under an inverted phase-contrast microscope (Olympus, magnification x100). The fourth-generation Hem-SCs were digested with 0.25% trypsin (Takara, Dalian, China) and centrifuged at 1000 g for 5 min. After washing twice with phosphate-buffered saline (PBS, Gibco, Waltham, MA, USA), they were resuspended in blocking buffer (BSA, Gibco) and stained with FITC-conjugated antibodies against human CD90 (cat. no. #A14728; eBioscience; San Diego, CA, USA), CD29 (cat. no. #14-0299-82; eBioscience), CD105 (cat.n o. #12-1057-42;

eBioscience), CD34 (cat. no. #12-0349-42; eBioscience) and CD45 (cat. no. #11-0459-42; eBioscience) antibodies for 10 min at 4°C. The stained cells were washed twice with PBS and detected by flow cytometry (BD Biosciences, San José, CA, USA) and analyzed with WinMDI software (v2.9).

Proliferation assay

Hem-SCs were implanted in 96-well plates (Corning Inc., Corning, NY, USA) at a density of 2,000~3,000 cells per well. 0, 2.5, 5, and 10 μmol/L of DAPT (Beyotime Biotechnology) were then added. DAPT was dissolved in dimethyl sulfoxide (DMSO, Beyotime Biotechnology). The final concentration of DMSO in the medium was 0.1%. Hem-SCs were cultured for 72 h, and then CCK-8 reagent (Dojindo, Tokyo, Japan) was added. Absorbance at 490 nm was measured using a microplate reader (Biotek ELx 800; BioTek Instruments, Inc., Winooski, VT, USA). Hem-SCs were implanted in 96-well plates at the density of 1,500~2,000 cells per well. They were treated with 5 μmol/L DAPT. CCK-8 reagent was added after 0, 1, 3, 5, and 7 days of culture, and the cells were cultured at 37°C for another 4 h. Absorbance readings at 490 nm were recorded using a microplate reader.

Western blot

0, 2.5, 5, and 10 μmol/L DAPT were added to Hem-SCs. The solution was changed every day and cultured for 72 h. When the Hem-SCs were confluent, the original medium was replaced with adipogenic medium (GUXMX-90031; Cyagen Biosciences, Santa Clara, CA, USA) , 5 μmol/L DAPT and DMSO with the same concentration were added, and cultured for 7 days. The medium was sucked and Hem-SCs were washed with PBS three times. Protein lysates (Servicebio, Wuhan, China) were added to extract the total protein of cells and the protein concentrations were detected. The separation was performed using an 8% polyacrylamide gel (Servicebio) by vertical electrophoresis. Then, the protein sample was transferred to a poly-vinylidene fluoride membrane (Servicebio) and sealed with 5% skimmed milk (Servicebio) at room temperature for 1 h. The following primary antibodies (Cell Signaling Technology, Inc., Danvers, MA, USA) were added overnight at 4°C. The following primary antibodies were used: Anti-NICD (cat. no. 3608, 1:1,000), Anti-Hes1 (cat. no. 11988, 1:1,000), Anti-VEGFR1 (cat. no. 64094, 1:1,000), Anti-VEGFR2 (cat. no. 9698, 1:1,000), Anti-VEGFR3 (cat. no. 33566, 1:1,000), Anti-p-PI3K (cat. no. 17366, 1:1,000), Anti-PI3K (cat. no. 4288, 1:1,000), Anti-p-AKT (cat. no. 9271, 1:1,000), Anti-AKT (cat. no. 9272, 1:1,000) and anti-β-actin (cat. no. 3700, 1:1,000). On the next day, it was washed with PBS three times at room temperature. Then the secondary antibody (cat. no. 7074; 1:2,000; Cell Signaling Technology, Inc.) was added for 1 h incubation. Finally, a chemiluminescence (Servicebio) solution was added for exposure and development.

Oil Red O staining

Hem-SCs were implanted in 6-well plates (Corning Inc.) at a density of 50,000 cells per well. When the cells were confluent, the original medium was replaced with an adipogenic medium and 5 μmol/L DAPT, 10 μmol/L PI3K/AKT signaling pathway agonist 740Y-P (Beyotime Biotechnology, dissolved in DMSO) and DMSO with the same concentration, were added. After 14 days of cell cultivation, the cells in each group were fixed with 2 mL 4% paraformaldehyde (Beyotime Biotechnology) for 30 min, rinsed with tri-distilled water 3 times and 60% isopropanol (Beyotime Biotechnology) for 1 time. One (1) mL of Oil Red O working solution (Beyotime Biotechnology) was added to each well to stain at room temperature for 20 min. After washing with tri-distilled water 2 times, the cells were observed under the microscope (Olympus, magnification 100×), and images were taken (Nikon Corporation, Tokyo, Japan). For semi-quantitative analysis, Oil Red O-stained cells were extracted with 1 mL isopropanol per well (15 min incubation). The eluate was transferred to 96-well plates (n=5 technical replicates per sample), and absorbance at 490 nm was measured using a microplate reader. Mean values were calculated for statistical analysis.

RT-qPCR

Total RNA was extracted by the Trizol (Thermo Fisher Scientific). The purity and concentration of the total RNA were detected by using NanoDrop 2000 spectrophotometer (Thermo Fisher Scientific). cDNA was synthesized by reverse transcription of 1 μg of total RNA using a PrimeScript™ RT kit (Takara). The cycling program consisted of a preliminary denaturation (90˚C for 10 min), followed by 45 cycles (90°C for 15 sec and 55°C for 1 min). The data were obtained and analyzed by ABI7500 real-time fluorescence quantitative PCR instrument (Applied Biosystems, Foster City, CA, USA). Glyceraldehyde-3-phosphate dehydrogenase (GAPDH) was used as an internal reference gene for standardization, and the $2^{\Delta\Delta CT}$ method was used for relative quantitative calculation. Primers for qPCR assays were from GenScript Biotech Company (Nanjing, China) and their sequences are shown in Table 1.

Statistical analyses

Data were expressed as the mean ±SEM (n=10 for each experiment). SPSS 23.0 (IBM Corp., Armonk, NY, USA) were used for statistical analyses. An unpaired Student's *t*-test was used to assess the differences in comparing the two groups, and analysis of variance was applied for the analysis of the mean values among multiple groups. A value of $p<0.05$ was considered significant.

Table 1. Sequences of primers used for qPCR.

Gene	Forward	Reverse
Notch1	CAAGAATGGTGCCAAGTGCC	AAGCAGAGGTAGGCGTTGTC
Jagged1	CGGGAAGTGCAAGAGTCAGT	TTGGTTTCACAGTAGGCCCC
Hes1	CCCAACGCAGTGTCACCTTC	TACAAAGGCGCA ATCCAATATG
PRAR-γ	ACCAAAGTGCAATCAAAGTGGA	ATGAGGGAGTTGGAAGGCTCT
C/EBPα	GGTGGACAAGAACAGCAACGAGT	CCAGCACCTTCTGCTGCGTCT
GAPDH	CATGTTCGTCATGGGGTGAACCA	AGTGATGGCATGGACTGTGGTCAT

Results

Morphological observation and identification of Hem-SCs

Isolated cells exhibited fibroblast-like morphology with irregular spindle shapes and cytoplasmic processes (Figure 1c). Flow cytometry confirmed mesenchymal stem cell immunophenotype: positive for CD29 (97.8%), CD90 (93.1%), and CD105 (88.7%); negative for hematopoietic markers CD34 (1.11%) and CD45 (0.69%) (Figure 1d).These observations preliminarily confirmed that the isolated cells were Hem-SCs.

DAPT inhibits the expression of the Notch signaling pathway in Hem-SCs

To determine if DAPT inhibits Notch signaling in Hem-SCs, cells were treated with DAPT (0, 2.5, 5.0, or 10.0 μM). Western blot analysis demonstrated dose-dependent Notch suppression: 5.0 and 10.0 μM DAPT significantly reduced NICD and Hes1 protein levels (p<0.01), confirming effective Notch pathway inhibition (Figure 2).

DAPT promotes proliferation of Hem-SCs

CCK-8 analysis demonstrated significant proliferation enhancement in Hem-SCs treated with 5.0 (p<0.01) and 10.0 (p<0.05) μM DAPT, and DAPT at 5.0 μM exhibited the highest

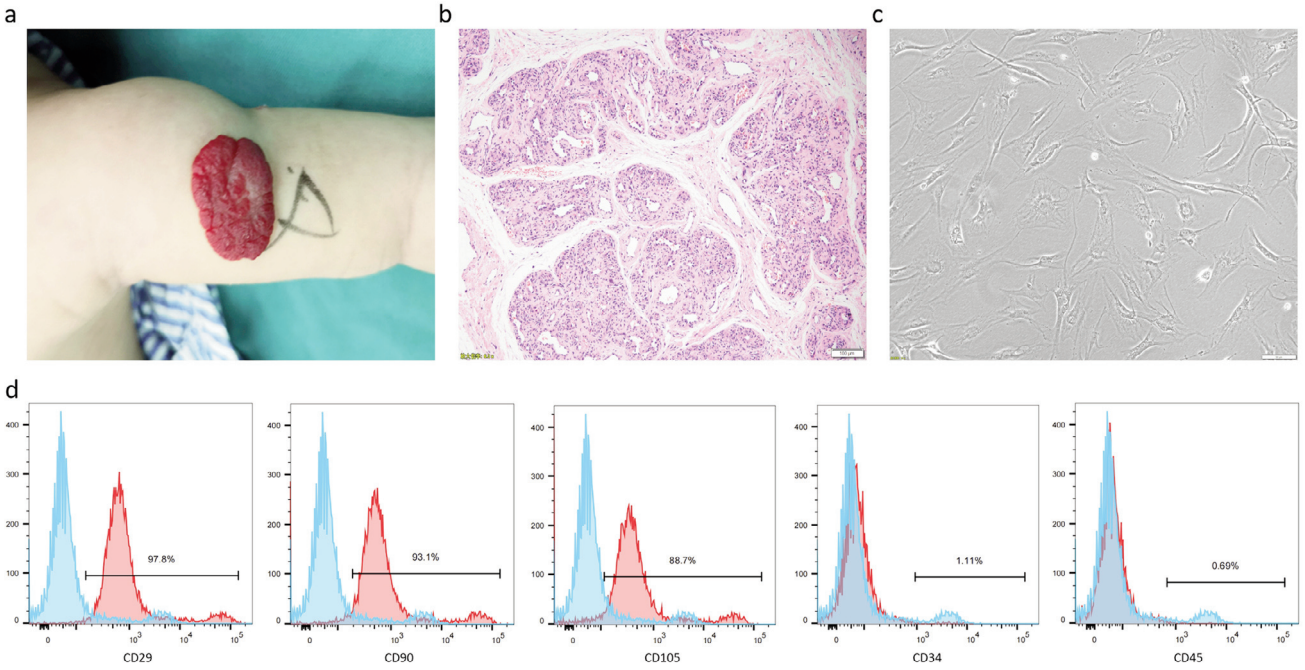

Figure 1. Morphological observation and identification of Hem-SCs. **a**) 4-mouth-old male children with hemangioma. **b**) Proliferative hemangioma; hematoxylin and eosin staining, magnification×100) **c**) The 4th generation cells of Hem-SCs under the inverted phase contrast microscope ; magnification 100×. **d**) Hem-SCs express CD29 (97.8%), CD90 (93.1%) and CD105 (88.7%), but do not express CD34 (1.11%) or CD45 (0.69%), according to flow cytometry.

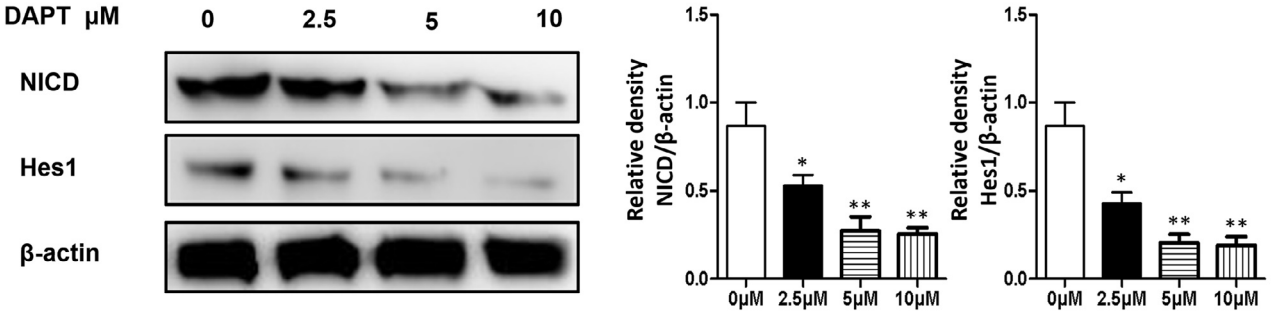

Figure 2. DAPT inhibits the expression of the Notch signaling pathway in Hem-SCs. Compared with the control group, 5.0 and 10.0 μM DAPT groups significantly inhibited the expressions of NICD and Hes1, which effectively blocked the Notch signaling in Hem-SCs. All data presented as mean± SEM, n=10; *p<0.05, **p<0.01 *vs* 0 μM group.

proliferation activity among all groups (p<0.05; Figure 3a). Growth curve quantification revealed sustained proliferative promotion in the 5.0 μM DAPT group from days 3-7 compared to untreated and vehicle controls (p<0.01; Figure 3b).

DAPT differentially regulates VEGFR expression in Hem-SCs

Western blot analysis revealed that pharmacological inhibition of Notch signaling by DAPT in Hem-SCs significantly downregulated VEGFR1 expression (p<0.01), upregulated VEGFR2 (p<0.01), and exerted no significant effect on VEGFR3 levels (Figure 4).

Adipogenic differentiation of Hem-SCs suppressed Notch signaling activity

RTqPCR analysis revealed significant downregulation of Notch1, Jagged1, and Hes1 transcript levels in Hem-SCs following 14-day adipogenic induction compared to non-induced controls (p<0.01; Figure 5).

DAPT potently enhances adipogenic differentiation of Hem-SCs

Oil Red O staining and semi-quantitative analysis confirmed successful adipogenic differentiation of Hem-SCs by day 14, evidenced by cytoplasmic lipid droplet accumulation in induced groups *versus* non-induced controls (Figure 6a). No significant difference was observed between the adipogenic induction group and DMSO vehicle control (p>0.05), ruling out solvent effects on differentiation. Notably, DAPT supplementation during adipogenic induction significantly enhanced lipid droplet formation compared to both standard induction and DMSO groups (p<0.01). Consistent with these findings, qPCR analysis demonstrated markedly elevated mRNA levels of adipogenic markers PPARγ and C/EBPα in DAPT-treated cells *versus* controls (p<0.01; Figure 6b).

DAPT suppresses PI3K/AKT signaling activity in Hem-SCs

Western blot analysis demonstrated that DAPT-mediated Notch inhibition significantly reduced the p-PI3K/PI3K and p-AKT/AKT ratios compared to the DMSO vehicle control (p<0.05). These findings indicate that DAPT suppresses PI3K/AKT signaling activity by attenuating PI3K and AKT phosphorylation (Figure 7).

740Y-P reverses DAPT-mediated adipogenic enhancement in Hem-SCs

The semiquantitative analysis of the Oil Red O-staining of the

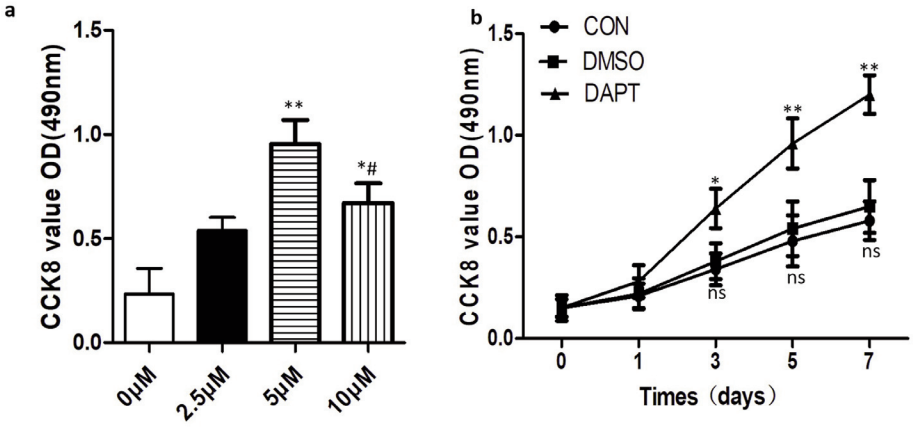

Figure 3. DAPT promotes proliferation of Hem-SCs. **a**) DAPT at 5.0 and 10.0 μM significantly promoted the proliferation of Hem-SCs as compared with the control group, and DAPT at 5.0 μM exhibited the highest proliferation activity among all groups. *p<0.05, ** p<0.01 *vs* 0 μM group; #p<0.05 *vs* 5.0 μM group. **b**) The proliferation of DAPT-treated Hem-SCs (days 3-7) was enhanced compared with the untreated group, and there was no significant difference in proliferation between the DMSO and control groups. All data presented as mean ±SEM, n=10. ns, no significance; *p<0.05, **p<0.01 *vs* control group.

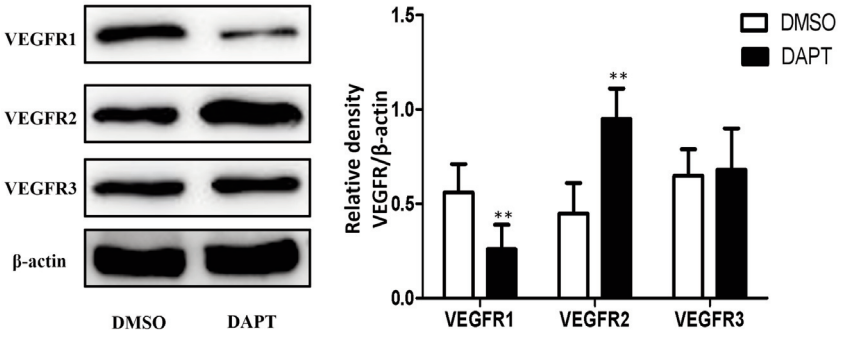

Figure 4. DAPT differentially regulates VEGFR expression in Hem-SCs. Western blot analysis demonstrated that DAPT-mediated Notch inhibition reciprocally regulated VEGFR expression in Hem-SCs: significantly downregulating VEGFR1 (p<0.01), upregulating VEGFR2 (p<0.01), while maintaining unchanged VEGFR3 levels. All data presented as mean ±SEM, n=10; **p<0.01 *vs* DMSO group.

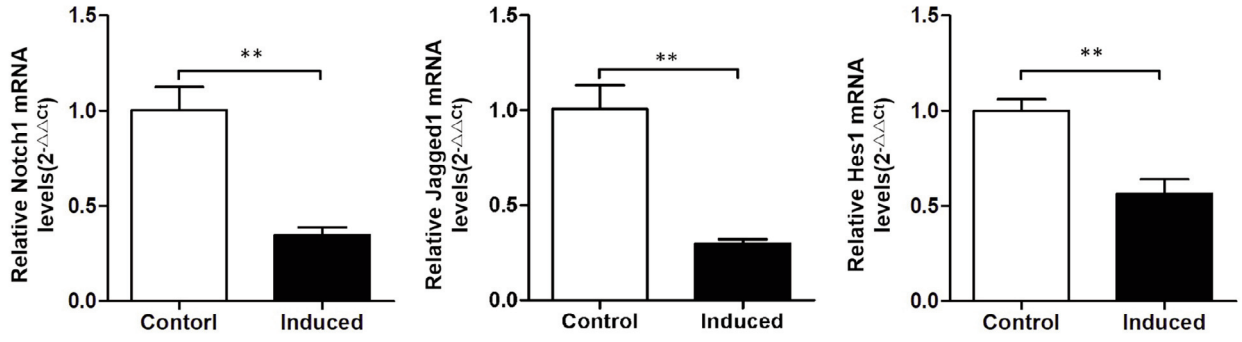

Figure 5. Adipogenic differentiation of Hem-SCs suppressed Notch signaling activity. The relative gene expressions of Notch1, Jagged1 and Hes1 were lower than those of the non-induced group at 14 days after adipogenic induction of Hem-SCs. All data presented as mean ±SEM, n=10; ***p*<0.01 *vs* control group.

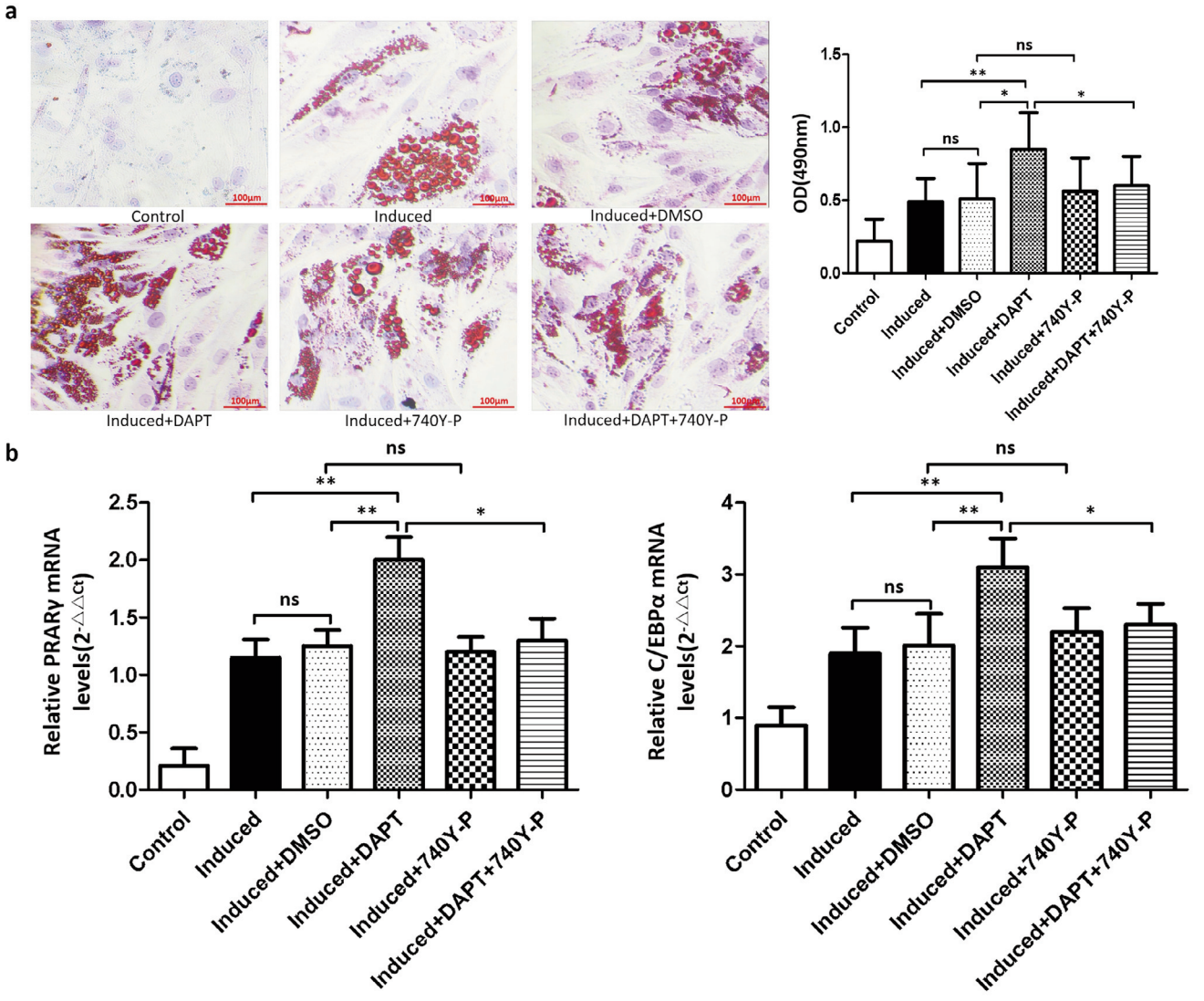

Figure 6. DAPT promotes whereas 740Y-P blocks the differentiation of Hem-SCs into fat cells. **a**) The Oil Red O-staining and the subsequent semi-quantitative analysis showing the effects of DAPT and 740Y-P on the adipogenic differentiation of Hem-SCs on the 14th day. **b**) RTqPCR showing the effects of DAPT and 740Y-P on the mRNA levels of PPARγ and C/EBPα during adipogenic differentiation of Hem-SCs on the 14th day. All data presented as mean ±SEM, n=10; ns, no significance, **p*<0.05, ***p*<0.01.

cells revealed that after adding 740Y-P (PI3K/AKT agonist) during the adipogenic induction of Hem-MSCs, the adipogenic effect was similar to the simple adipogenic induction and the DMSO groups with no significant difference($p>0.05$). After adding DAPT and 740Y-P, compared with the DAPT group, the formation of red lipid droplets in the cytoplasm decreased ($p<0.05$), similar to that in simple adipogenic induction and the DMSO groups (Figure 5). RTqPCR results revealed that after adding 740Y-P, the mRNA levels of fat cell markers of PPARγ and C/EBPα were similar to that in the simple adipogenic induction and the DMSO groups. After adding DAPT and 740Y-P, compared with the DAPT group, the gene expressions of PRARγ and C/EBPα decreased, similar to simple adipogenic induction and the DMSO groups (Figure 5).

Discussion

The natural progression of IH encompasses stage-specific histopathological restructuring, as evidenced by hematoxylin-eosin analysis of lesional tissues. Proliferative-phase IH exhibits hypercellular endothelial clusters forming primitive microvascular channels, whereas involution-phase lesions demonstrate progressive endothelial apoptosis, microvascular occlusion, and ultimate adipose replacement.[19] This morphological continuum establishes angiogenesis and adipogenic differentiation as dual cornerstones of the IH pathogenetic process that our study mechanistically deciphers through Notch/PI3K/AKT axis modulation in Hem-SCs.

Accumulating evidence identifies Hem-SCs as central drivers of IH pathobiology.[20,21] Hem-SCs function as IH progenitor cells that recapitulate the disease's proliferative-regressive cycle in xenograft models.[22] Their pathological significance arises from Notch-mediated lineage plasticity: Jagged1 promotes endothelial/pericyte differentiation to facilitate angiogenesis, whereas Notch3 maintains vascular stability-genetic ablation of Notch3 induces vascular collapse and suppresses lesion progression.[23,24] This dual regulatory mechanism establishes Hem-SCs as orchestrators of IH's characteristic transition from hypervascular proliferation to adipose involution.

Dose-response analysis identified 5 μmol/L DAPT as the optimal concentration for Notch inhibition in Hem-SCs, subsequently applied throughout this study. CCK-8 assays revealed biphasic proliferation kinetics: initial growth suppression (day 1, potentially due to low-density paracrine limitations) followed by accelerated exponential proliferation from day 3 onward, demonstrating DAPT's potent mitogenic effect.

IH, a proliferative vascular endothelial tumor, is critically regulated by VEGF signaling with elevated ligand levels during proliferation.[25] HemECs exhibit pathogenic VEGFR dysregulation (↓VEGFR1/↑VEGFR2), while Notch ligand DLL4 (Delta-like ligand 4) serves as a tumor angiogenesis suppressor.[26,27] Paradoxically, DLL4 blockade increases vascular density but generates dysfunctional neovessels (narrow lumens, poor perfusion), ultimately reducing tumor volume through nutrient deprivation.[28]

Western blot analysis demonstrated that Notch inhibition by DAPT reciprocally modulates VEGFR expression in Hem-SCs: suppressing VEGFR1 while upregulating VEGFR2, with VEGFR3 unchanged. This reveals cross-regulation between Notch and VEGF pathways–a feedback loop coordinating vascular development. Paradoxically, VEGFR2-driven endothelial proliferation generates malformed vasculature (luminal stenosis, impaired perfusion), ultimately disrupting metabolic supply and suppressing IH progression through vascular insufficiency.

Notch signaling suppresses adipogenesis in mesenchymal SCs.[29] We further assessed Notch signaling dynamics during Hem-SC adipogenesis *via* RTqPCR. Following adipogenic induction, the expression of Notch1, Jagged1, and Hes1 significantly decreased compared to non-induced controls, indicating that Notch pathway suppression facilitates adipocyte commitment. Crucially, DAPT-mediated Notch inhibition during adipogenic induction markedly enhanced differentiation: both Oil Red O-staining (lipid accumulation) and adipogenic markers (PPARγ, C/EBPα) were significantly upregulated *versus* standard induction and DMSO vehicle groups. These results confirm Notch blockade promotes robust adipocyte differentiation in Hem-SCs.

The PI3K/AKT pathway critically regulates cellular physiology and pathology,[30] demonstrating multifaceted crosstalk with Notch signaling: Notch-PI3K/AKT dysregulation drives T-cell leukemogenesis;[31] NICD activates PI3K/AKT via CBF-1 binding on MVP promoter;[32] while Notch inhibition suppresses PI3K/AKT through Hes1-mediated PTEN derepression,[33] establishing an interconnected regulatory axis.

Western blot analysis of DAPT-treated Hem-SCs undergoing adipogenic differentiation revealed decreased p-PI3K/PI3K and p-AKT/AKT ratios, demonstrating Notch inhibition suppresses PI3K/AKT signaling activity during adipocyte commitment.

To determine whether DAPT's pro-adipogenic effect involves

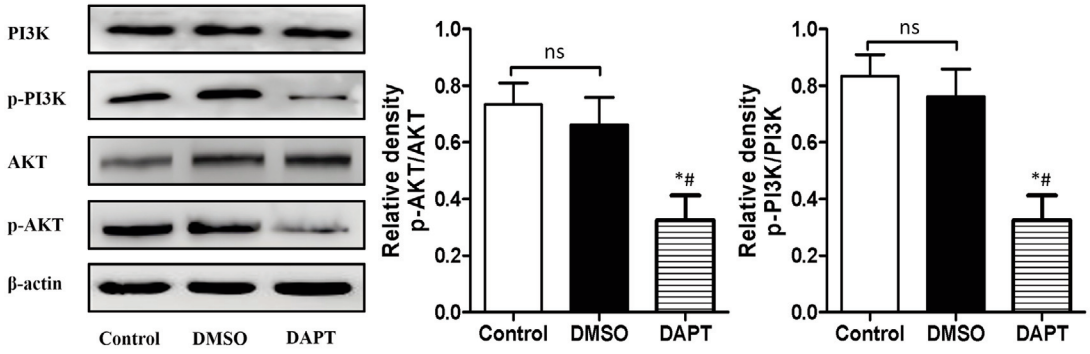

Figure 7. DAPT suppresses PI3K/AKT signaling activity in Hem-SCs. Western blot showed that after DAPT was added to the Hem-SCs to block the Notch signaling pathway, compared with the DMSO group, the p-PI3K/PI3K, p-AKT/AKT ratios decreased. All data presented as mean± SEM, n=10; ns, no significance, *$p<0.05$ *vs* control group; $^{\#}p<0.05$ *vs* DMSO group.

PI3K/AKT suppression in Hem-SCs, we co-administered DAPT with the PI3K activator 740Y-P during adipogenic induction. While 740Y-P alone did not inhibit adipogenesis, combined treatment with DAPT and 740Y-P significantly downregulated adipogenic markers PPARγ and C/EBPα mRNA, reverting to baseline levels observed in standard induction and DMSO controls. This functional rescue demonstrates that 740Y-P reverses DAPT-mediated adipogenic enhancement, confirming that DAPT promotes adipocyte differentiation through PI3K/AKT pathway inhibition.

Based on the above discussion, we demonstrate that Notch inhibition promotes Hem-SCs proliferation, angiogenesis, and adipocyte differentiation *via* PI3K/AKT suppression. Our study provides two novel mechanistic insights specific to IH pathogenesis: i) we demonstrated, for the first time, that Notch inhibition differentially regulates VEGFR subtypes (↓VEGFR1/↑VEGFR2) in Hem-SCs, uncoupling proliferation from functional vasculogenesis and driving dysfunctional vasculature; and ii) we validated, *via* 740Y-P rescue, that the PI3K/AKT pathway serves as the primary downstream effector of this Notch-mediated regulation. These findings collectively establish Notch-PI3K/AKT modulation as a promising mechanism-based therapeutic strategy for IH.

The present study has two key limitations: i) the functional heterogeneity among four Notch receptors (Notch1-4) and five ligands (Jagged1/2, DLL1/3/4) is still unresolved; and ii) the results *in vitro* require validation *in vivo*. Future studies should elucidate isoform-specific Notch functions, and explore therapeutic translation *via* Notch inhibition combined with pro-adipogenic stimuli.

Acknowledgements

We thank Cao Lei, Ph.D., for technical assistance. The authors would like to thank all reviewers who participated in the review, as well as MJEditor (www.mjeditor.com) for providing English editing services during the preparation of this manuscript.

References

1. Jung HL. Update on infantile hemangioma. Clin Exp Pediatr. 2021;64:559-72.
2. Lewis D, Vaidya R. Congenital and infantile hepatic hemangioma. StatPearls. Treasure Island, StatPearls Publishing; 2025.
3. Kowalska M, Dębek W, Matuszczak E. Infantile hemangiomas: An update on pathogenesis and treatment. J Clin Med 2021;10:4631.
4. Sharma A, Gupta M, Mahajan R. Infantile hemangiomas: a dermatologist's perspective. Eur J Pediatr 2024;183:4159-68.
5. Xiang S, Gong X, Qiu T, Zhou J, Yang K, Lan Y, et al. Insights into the mechanisms of angiogenesis in infantile hemangioma. Biomed Pharmacother 2024;178:117181.
6. Rešić A, Barčot Z, Habek D, Pogorelić Z, Bašković M. The Evaluation, diagnosis, and management of infantile hemangiomas - A comprehensive review. J Clin Med 2025;14:425.
7. Tian Z, Yu T, Liu J, Wang T, Higuchi A. Introduction to stem cells. Prog Mol Biol Transl Sci 2023;199:3-32.
8. Tan JWH, Wylie-Sears J, Seebauer CT, Mulliken JB, Francois M, Holm A, et al. R(+) Propranolol decreases lipid accumulation in hemangioma-derived stem cells. bioRxiv 2024;2024.07.01.601621.
9. Zinellu A, Mangoni AA. Vascular endothelial growth factor as a potential biomarker in systemic sclerosis: a systematic review and meta-analysis. Front Immunol 2024;15:1442913.
10. Yu E, Kim H, Park H, Hong JH, Jin J, Song Y,et al. Targeting the VEGFR2 signaling pathway for angiogenesis and fibrosis regulation in neovascular age-related macular degeneration. Sci Rep 2024;14:25682.
11. Mukherjee T, Pattnaik A, Sahu SS. Analyzing VEGFA/VEGFR1 Interaction: application of the resonant recognition model-stockwell transform method to explore potential therapeutics for angiogenesis-related diseases. Protein J 2024;43:697-710.
12. Zhou B, Lin W, Long Y, Yang Y, Zhang H, Wu K, et al. Notch signaling pathway: architecture, disease, and therapeutics. Signal Transduct Target Ther 2022;7:95.
13. Reichrath J, Reichrath S. Notch pathway and inherited diseases: Challenge and promise. In: Reichrath J, Reichrath S, editors. Notch signaling in embryology and cancer. Cham, Springer; 2020. pp. 159-87.
14. Zhang H, Wei T, Johnson A, Sun R, Richter G, Strub GM. NOTCH pathway activation in infantile hemangiomas. J Vasc Surg Venous Lymphat Disord 2021;9:489-96.
15. Glaviano A, Foo ASC, Lam HY, Yap KCH, Jacot W, Jones RH, et al. PI3K/AKT/mTOR signaling transduction pathway and targeted therapies in cancer. Mol Cancer 2023;22:138.
16. Chen L, Liu Y, Wang Z, Zhang L, Xu Y, Li Y, et al. Mesenchymal stem cell-derived extracellular vesicles protect against abdominal aortic aneurysm formation by inhibiting NET-induced ferroptosis. Exp Mol Med 2023;55:939-51.
17. Ke C, Chen C, Yang M, Chen H, Ke Y, Li L. Inhibition of infantile hemangioma growth and promotion of apoptosis via VEGF/PI3K/AKT axis by 755-nm long-pulse alexandrite laser. Biomed J 2024;47:100675.
18. Gui Y, Wang L, Huang Z. MiR-137 inhibits cervical cancer progression via down-modulating Notch1 and inhibiting the PI3K/AKT/mTOR signaling pathway. Transl Cancer Res 2021;10:3748-56.
19. Vo K, Amarasinghe B, Washington K, Gonzalez A, Berlin J, Dang TP. Targeting notch pathway enhances rapamycin antitumor activity in pancreas cancers through PTEN phosphorylation. Mol Cancer 2011;10:138.
20. Harter N, Mancini AJ. Diagnosis and Management of infantile hemangiomas in the neonate. Pediatr Clin North Am 2019;66:437-59.
21. Wu P, Xu H, Li N, Huo R, Shen B, Lin X, et al. Hypoxia-induced Cyr61/CCN1 production in infantile hemangioma. Plast Reconstr Surg 2021;147:412e-423e.
22. Maimaiti A, Aierken Y, Zhou L, He J, Abudureyimu A, Li SX. Inhibiting interleukin-6/signal Transducers and activators of transduction-3/Hypoxia-inducible factor-1α signaling pathway suppressed the growth of infantile hemangioma. Eur J Pediatr Surg 2023;33:158-66.
23. Khan ZA, Boscolo E, Picard A,Psutka S, Melero-Martin JM, Bartch TC, et al. Multipotential stem cells recapitulate human infantile hemangioma in immunodeficient mice. J Clin Invest 2008;118:2592-9.
24. Boscolo E, Stewart CL, Greenberger S, Wu JK, Durham JT, Herman IM, et al. JAGGED1 signaling regulates hemangioma stem cell-to-pericyte/vascular smooth muscle cell differentiation. Arterioscler Thromb Vasc Biol 2011;31:2181-92.
25. Edwards AK, Glithero K, Grzesik P, Kitajewski AA, Munabi NCO, Hardy K, et al. NOTCH3 regulates stem-to–mural cell differentiation in infantile hemangioma. JCI Insight 2017;2:e93764.
26. Makkeyah SM, Elseedawy ME, Abdel-Kader HM, Mokhtar GM, Ragab IA. Vascular endothelial growth factor response with propranolol therapy in patients with infantile hemangioma. Pediatr Hematol Oncol 2022;39:215-24.
27. Peng J, Li F, Qiu M, Xu X, Liu G, Ou J. Inhibition of hemangioma development by regulating the VEGF/VEGFR autocrine loop via the miR-494/PTEN pathway. Discov Oncol 2025;16:168.
28. Jin F, Guan P, Huang L, Zhang A, Gao S, Wang L, et al. DLL4/VEGF bispecific molecularly imprinted nanomissile for robust tumor therapy. Biomaterials 2025;322:123412.
29. Semenova D, Bogdanova M, Kostina A, Golovkin A, Kostareva A, Malashicheva A. Dose-dependent mechanism of Notch action in promoting osteogenic differentiation of mesenchymal stem cells. Cell Tissue Res 2020;379:169-79.
30. Liu B, Wang D, Xiong T, Liu Y, Jing X, Du J,et al. Inhibition of Notch signaling promotes the differentiation of epicardial progenitor cells into adipocytes. Stem Cells Int 2021;2021:8859071.

31. Teng Y, Fan Y, Ma J, Lu W, Liu N, Chen Y, et al. The PI3K/AKT pathway: Emerging roles in skin homeostasis and a group of non-malignant skin disorders. Cells 2021;10:1219.
32. Raetz EA, Teachey DT. T-cell acute lymphoblastic leukemia. Hematology 2016;2016:580-8.
33. Xiao YS, Zeng D, Liang YK, Wu Y, Li MF, Qi YZ, et al. Major vault protein is a direct target of Notch1 signaling and contributes to chemoresistance in triple-negative breast cancer cells. Cancer Lett 2019;440-441:156-67.

Received: 2 June 205. Accepted: 28 July 2025.

European Journal of Histochemistry 2025; 69:4241
doi:10.4081/ejh.2025.4241